

# Picosecond-resolution soft-x-ray laser plasma interferometry

Jorge Filevich, Jorge J. Rocca, Mario C. Marconi, Raymond F. Smith, James Dunn, Roisin Keenan, James R. Hunter, Stephen J. Moon, Joseph Nilsen, Andrew Ng, and Vyacheslav N. Shlyaptsev

We describe a soft-x-ray laser interferometry technique that allows two-dimensional diagnosis of plasma electron density with picosecond time resolution. It consists of the combination of a robust high-throughput amplitude-division interferometer and a 14.7-nm transient-inversion soft-x-ray laser that produces  $\sim 5$ -ps pulses. Because of its picosecond resolution and short-wavelength scalability, this technique has the potential for extending the high inherent precision of soft-x-ray laser interferometry to the study of very dense plasmas of significant fundamental and practical interest, such as those investigated for inertial confinement fusion. Results of its use in the diagnostics of dense large-scale laser-created plasmas are presented. © 2004 Optical Society of America

OCIS codes: 350.5400, 140.7240, 120.3180, 340.7450.

## 1. Introduction

Since the advent of optical lasers, interferometry has been widely used to study different types of plasmas.<sup>1</sup> This powerful technique provides information in the form of two-dimensional maps of the electron density, often without the need of extensive modeling. However, when the plasma density approaches a fraction of a percent of the critical density, refraction and opacity effects can significantly limit these kind of diagnostics.<sup>2</sup> Refraction that is due to steep density gradients in the plasma can steer the probe beam completely out of the plasma, limiting the maximum plasma density and size that can be studied. In addition, at high plasma densities, free-free absorption

can attenuate the probe beam, obscuring part of the interferogram. Nevertheless, both of these adverse effects can be greatly reduced by significant shortening of the wavelength of the probe beam. This constitutes the main motivation for pursuing soft-x-ray laser interferometry. Soft-x-ray lasers with wavelengths corresponding to critical densities in the range of  $5 \times 10^{23}$ – $5 \times 10^{24}$  cm<sup>-3</sup> can potentially probe plasmas with densities up to 2 orders of magnitude larger than those accessible with optical lasers. In addition, x-ray lasers can provide the high brightness necessary to overcome the intense radiation emitted by hot dense plasmas.

The first demonstrations of soft-x-ray plasma interferometry were performed with a 15.5-nm Ne-like Y laser pumped by the laboratory-size Nova laser. In these initial proof-of-principle experiments, Da Silva *et al.*<sup>3</sup> and Celliers *et al.*<sup>4</sup> demonstrated a Mach-Zehnder interferometer based on multilayer-coated thin-film beam splitters. With this interferometer, large (1-mm scale) plasmas were probed as close as 25  $\mu$ m from the initial target surface, where the electron density reached  $2 \times 10^{21}$  cm<sup>-3</sup>. More recently, the versatility of soft-x-ray laser interferometry was increased with the development of tabletop lasers with peak spectral brightness that equals or exceeds that of their laboratory-size predecessors.<sup>5,6</sup> Interferometry experiments performed at Colorado State University took advantage of a high-repetition-rate tabletop capillary discharge pumped 46.9-nm laser<sup>5</sup> to obtain sequences of interferograms that map the

---

J. Filevich (rage@engr.colostate.edu), J. J. Rocca, and M. C. Marconi are with the National Science Foundation Engineering Research Center for Extreme Ultraviolet Science and Technology and Department of Electrical and Computer Engineering, Colorado State University, Fort Collins, Colorado 80523. R. F. Smith, J. Dunn, R. Keenan, J. R. Hunter, S. J. Moon, J. Nilsen, and A. Ng are with the Lawrence Livermore National Laboratory, Livermore, California 94550. V. N. Shlyaptsev is with the Department of Applied Science, University of California Davis-Livermore, Livermore, California 94550. M. C. Marconi's permanent address is Department of Physics, University of Buenos Aires, Buenos Aires, Argentina.

Received 29 October 2003; revised manuscript received 2 March 2004; accepted 2 April 2004.

0003-6935/04/193938-09\$15.00/0

© 2004 Optical Society of America

evolution of laser-created plasmas. Initial studies made use of a Lloyd's mirror interferometer,<sup>7,8</sup> and subsequent experiments used an amplitude-division interferometer based on diffraction gratings.<sup>9</sup> However, the relatively long duration of the soft-x-ray laser pulses used in these demonstrations (300 ps and 1.2 ns for the Ne-like Y and Ne-like Ar lasers, respectively) makes the interferograms susceptible to the blurring of the interference fringes that results from the rapid local variations of the electron density during the exposure time within a fast-moving plasma. Although these pulse widths are adequate for mapping the density of numerous slowly evolving dense plasmas, such as pulse-power plasmas and laser-created plasmas far from the target surface, it precludes their use in diagnosing plasmas in which fast-evolving steep density gradients lead to blurring of the fringes.

In this paper we describe a soft-x-ray laser interferometry technique<sup>10</sup> that is capable of picosecond-resolution plasma probing, which overcomes the limitations imposed by the rapid plasma motion. It consists of the combination of a robust high-throughput amplitude-division interferometer and a 14.7-nm laser that produces ~5-ps pulses. The interferometer is a modification of the diffraction-grating interferometer (DGI) used in the capillary discharge soft-x-ray laser interferometry experiments. It combines the advantages of increased resistance to damage by plasma debris with a high throughput of 6% per arm. The picosecond soft-x-ray laser probe is the saturated output of the 14.7-nm Ni-like Pd transient-inversion scheme.<sup>6</sup> Both the DGI and the transient-inversion laser are scalable to significantly shorter wavelengths (e.g., by use of the 7.36-nm line of Ni-like Sm<sup>11</sup>). This scalability, when combined with the picosecond resolution of this technique, has the potential for extending the high inherent precision of soft-x-ray laser interferometry to the study of very dense plasmas of significant fundamental and practical interest, such as those investigated for inertial confinement fusion. The next section briefly reviews several designs of soft-x-ray laser interferometers and describes the DGI design and its alignment procedure. Section 3 presents results of dense plasma diagnostics that utilize this picosecond-resolution soft-x-ray laser interferometry technique.

## 2. Soft-X-Ray Laser Interferometers

The main limitation in the construction of interferometers for the soft-x-ray region of the spectrum has been the development of adequate amplitude-division beam splitters. Another limiting factor is the availability of mirrors with sufficiently high reflectivity to achieve a useful throughput. The amplitude-division beam splitters can be avoided if wave-front-division interferometers are used instead. In these schemes, the probe beam is divided spatially to provide the reference and probe arms of the interferometer. The reflectivity requirements can be met, in some cases, by use of grazing-incidence reflections, and in others, with high-reflectivity multi-

layer soft-x-ray mirrors. However, the wave-front-division interferometers have the drawback of a higher requirement on the spatial coherence of the laser source. This limitation can be overcome if the source is placed far away from the interferometer as, according to the Huygens-Fresnel principle,<sup>12</sup> the beam's transverse coherence increases with the distance from the source; however, this requires an increased photon fluence.

The simplest interferometer that can be constructed is based on Lloyd's mirror configuration.<sup>13</sup> This interferometer was implemented in combination with a soft-x-ray laser by Rocca *et al.*,<sup>7</sup> and it was used in the diagnostic of a pinch plasma.<sup>8</sup> It consists of a reflection in a grazing-incidence mirror that intercepts a portion of the beam from the soft-x-ray laser source. The fringe pattern arises from the superposition of this portion of the beam with the one that propagates directly from the source. Because of the single grazing reflection this interferometer has high throughput. The fringe spacing is determined by the angle of incidence and the distances from the point source to the mirror and from the mirror to the image plane. The plasma to be probed is placed in one of the two portions of the beam, and the other portion is used as a reference. The maximum transverse plasma size that can be probed is determined by the mirror length and the angle of incidence on the mirror and by the spatial and temporal coherence of the laser. The Fresnel bimirror interferometer<sup>13</sup> is almost as simple as the Lloyd's mirror. It consists of two flat mirrors joined together at one side with a slight tilt between them. The light incident at a grazing angle on the mirrors is reflected and, because of this tilt, is overlapped with itself, generating interference fringes. This interferometer was used in combination with a 21.2-nm Ne-like Zn soft-x-ray laser by Albert *et al.*<sup>14</sup> and was demonstrated in studying the effect of high electric fields on Nb surfaces.<sup>15</sup> Amplitude-division interferometers do not have the limitation on the spatial coherence of the laser source and can probe larger objects. The first amplitude-division soft-x-ray laser interferometry experiment was performed with a Ne-like Y 15.5-nm soft-x-ray laser pumped by the laboratory-size Nova laser. Da Silva *et al.* demonstrated the technique for plasma diagnostics by using an interferometer that utilized Mo-Si thin-film multilayer-coated beam splitters and mirrors mounted in a Mach-Zehnder configuration.<sup>16</sup> This interferometer was used to probe millimeter-scale plasmas at distances as close as 25  $\mu\text{m}$  from the initial target surface, where the measured electron density reached  $2 \times 10^{21} \text{ cm}^{-3}$ .<sup>3</sup> It was also used to perform studies of the coherence length of the soft-x-ray laser.<sup>4</sup> These experiments were the first to realize soft-x-ray interferometry of dense plasmas. However, the low repetition rate of the laboratory-size x-ray lasers used and the fragile beam splitters that had to be replaced after every shot limited the amount of data that could be taken. Furthermore, the 300-ps pulse duration of the probe laser limited the types of plasmas that could be studied because of

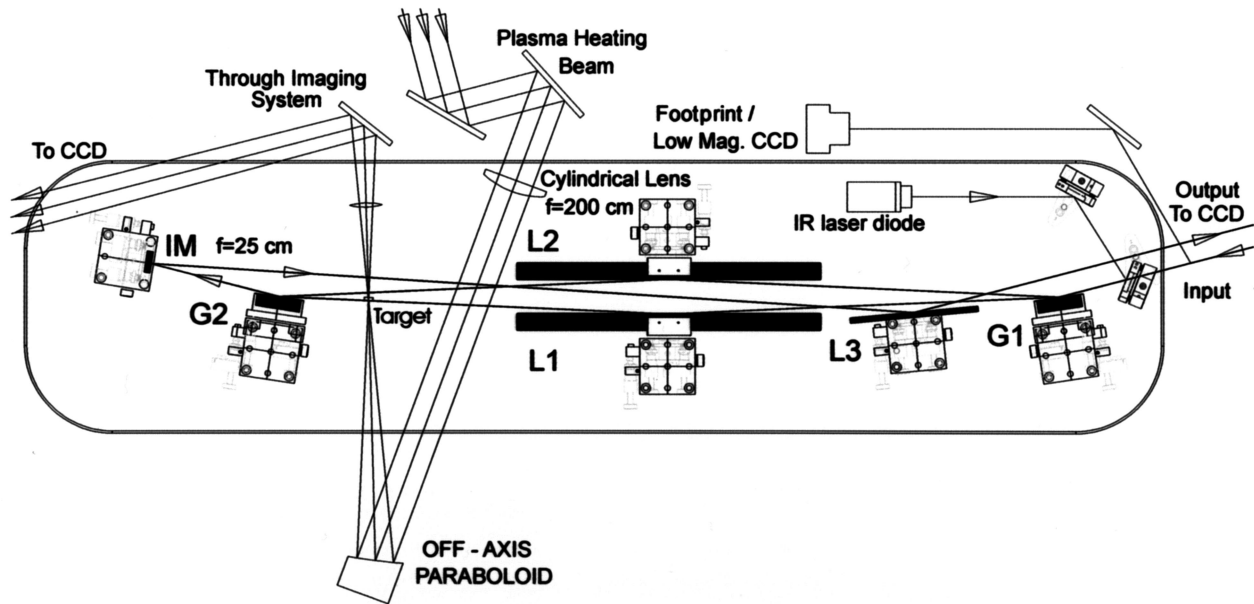


Fig. 1. Experimental setup showing the DGI. The soft-x-ray laser enters and exits the interferometer through the lower right-hand side. For definitions of notation used, please see text.

the possible blurring of the interference fringes. Another amplitude-division interferometer, a Michelson interferometer based on multilayer foil beam splitters that provided transmission and reflectivity of 15% and 14%, respectively, was recently constructed and used to measure the longitudinal coherence length of the Ni-like Pd 14.7-nm soft-x-ray laser.<sup>17</sup> The use of these types of instruments is limited to the wavelength range in which low-absorption thin-film multilayer beam splitters can be manufactured.

The interferometer used to implement the picosecond-resolution plasma-diagnostics tool described in this paper uses reflective diffraction gratings as beam splitters.<sup>9,18</sup> The use of diffraction gratings allows the construction of amplitude-division interferometers of increased robustness and high throughput that can be designed to operate over an extended range of soft-x-ray wavelengths. The DGI was first demonstrated in combination with a 46.9-nm capillary discharge soft-x-ray laser, and it was used to unveil two-dimensional phenomena in line-focus and spot-focus laser-created plasmas.<sup>19,20</sup> The DGI described in this paper is a modified version designed to operate at the 14.7-nm Ni-like Pd soft-x-ray laser wavelength with picosecond pulse duration. A description of this instrument, its alignment procedure, and its use for laser-created plasma diagnostics are given in the next sections.

### 3. Diffraction Grating Interferometer

The DGI is set in a skewed Mach-Zehnder configuration, as shown in Fig. 1. The light incident upon the first grating (G1) is diffracted with approximately equal intensity in the zero and first orders. These two beams that form the two arms of the interferometer are reflected at 2.6° grazing-incidence angle to-

ward a second 7.6 cm × 8.5 cm diffraction grating (G2) by two 35-cm-long Au-coated mirrors (L1 and L2). Grating G2 recombines the two beams such that they exit the interferometer, propagating with a small angular difference selected to produce fringes of the spacing required by the particular experiment. By simulation of the grating's performance,<sup>21</sup> a line spacing of 900 lines/mm and a blaze angle of 2° were chosen. This grating diffracts the beam into a zero-order component and a first-order component of approximately the same intensity when operating at an incidence angle of 6°. For the selected ruling and angle of incidence, the resulting angle between the zero and the first diffracted orders is 5.2°. This dispersion angle defines the geometry of the interferometer. Thus, with the two gratings separated by 90 cm center to center, the resulting distance between the two arms of the interferometer at the target position indicated in Fig. 1 is ~1 cm. The phase object of interest, in our case a laser-created plasma, is placed there. The reflectivity of the Au-coated diffraction gratings is maximized by the small grazing-incidence angle used, resulting in an efficiency of 25% per order on each grating. The long mirror's (L1 and L2) reflectivity is ~90%, giving a total throughput for the instrument, excluding the imaging optics, of ~12%.

Because of the wavelength-dependent dispersion of the gratings, the alignment of the interferometer cannot, in principle, be performed with an auxiliary optical laser. To overcome this difficulty the diffraction gratings are designed to have two different, vertically separated, ruled sections on the same substrate. The section associated with alignment has a line spacing chosen to produce the same dispersion for a selected infrared (IR) laser diode as the



dispersion of the soft-x-ray laser on its ruled section. This IR laser diode for alignment is chosen to have a temporal coherence length similar to or shorter than that of the soft-x-ray laser ( $\sim 400 \mu\text{m}$   $1/e$  HW).<sup>17</sup> This ensures that the arm lengths are matched with sufficient precision to warrant the observation of fringes with the soft x-ray laser. The laser diode chosen<sup>22</sup> has a central wavelength of 827 nm and an estimated coherence length of  $\sim 300 \mu\text{m}$ . This wavelength determines the line density of the alignment ruling to be 16 lines/mm. Specifically, the gratings have a central region with 900 lines/mm for the soft-x-ray laser radiation, and two other regions situated on top and below that have 16 lines/mm rulings to be used with the IR laser diode. This three-stripe ruling design permits the rotation of the second grating in order to reverse the blaze angle direction as is needed to recombine the two soft-x-ray laser beams with equal intensities. The soft-x-ray laser beam at the target position is imaged onto a  $1.33 \text{ cm} \times 1.33 \text{ cm}$  charge-coupled device (CCD) with  $1024 \times 1024$  pixels of  $13 \mu\text{m} \times 13 \mu\text{m}$  size.<sup>23</sup> The imaging optics consist of a 25-cm focal-length Mo-Si multilayer spherical imaging mirror (IM), set at  $5^\circ$  off normal incidence, followed by an elongated Au-coated mirror (L3), positioned at a grazing angle of  $9^\circ$  that relays the beam via a flat  $45^\circ$  Mo-Si multilayer mirror to the CCD detector located approximately 5.5 m away from the imaging mirror. This imaging setup has a total magnification of  $22\times$  that we measure by imaging a  $12.7\text{-}\mu\text{m}$  spacing mesh placed at the target plane position (object plane of IM). This means a single CCD pixel is equivalent to  $0.6 \mu\text{m}$  at the object plane, and the overall system spatial resolution is determined to be  $\sim 2 \mu\text{m}$ .

To align the DGI, a 632.8-nm He-Ne laser beam is first pointed along the input path of the soft-x-ray beam into the first grating. This visible beam is then steered with G1, L1, and G2 along the zero-order arm into the detector. The first-order alignment is then performed with the 16-lines/mm secondary ruling and the 827-nm IR laser diode. The IR laser diode is steered along the zero-order path by two Al-coated mirrors to ensure that the incidence angle on the first grating is correct. The first-diffracted-order beam is subsequently adjusted with L2 to follow the first-order arm of the interferometer. Final corrections of L2 and G2 are made until the fringes are clearly observed at the output of the DGI. At this stage of the alignment the orientation (vertical or horizontal) of the fringes can be chosen. Also, for its use in plasma diagnosis, it is usually advantageous to ensure that the angle between the beams is such that a plasma set on the zero-order beam will produce fringe shifts away from the target. This often facilitates the interpretation of the fringe shifts for the determination of the electron-density profile. Because the height of the IR beam is different from that of the soft-x-ray laser beam, the alignment through the imaging optics onto the detector is done with the visible He-Ne laser by use of the zero-order arm.

Because of the difficulty in obtaining a good blaze

profile on very small groove densities, the IR ruling is effectively not blazed. As a result, most of the IR energy is diffracted onto the zero-order arm, creating a large intensity difference between the two arms of the DGI, when aligning. This prevents the fringes from the IR alignment laser from being observed at the output of the DGI. However, the first diffracted order off the second grating can be used instead for this purpose. In this case the intensity of both orders is similar because each undergoes a reflection (zero-order) and a first-order diffraction. As the optimum alignment can differ slightly from that obtained with the IR beam the final adjustments are conducted under vacuum with the soft-x-ray laser beam, with motorized actuators to control the position of the relevant optics. We discovered that some of the movements are more critical than others. For example, it was found that there is no need to motorize G1. In contrast, the translations of L1 and L2 are important, and it is useful to have these axes encoded because they provide control of the overlap between the beams of the two arms. The horizontal and the vertical tilts of L2 and G2 are used frequently to orient the fringes and to select the desired fringe spacing. L1 vertical and horizontal tilts are used, but not as often as those on L2. The translation of G2 is also used but less frequently. It is important to have the IM translation motorized to be able to adjust the focus and produce a sharp image of the target on the detector. The horizontal and the vertical tilts of both this mirror and the relay mirror (L3) are used to steer the beam into the CCD camera, but it is possible to operate with only adjusting the relay mirror tilt if it is found that only small corrections are required.

The combination of a CCD camera placed inside the DGI chamber with two flip-in mirrors allowed the monitoring of the soft-x-ray laser beam at the input and at the output of the interferometer (see Fig. 1, "Foot Print/Low Mag. CCD"). In this way, the pointing of the soft x ray at the input of the DGI could be compared with that of the He-Ne laser used to align it. The relatively low magnification ( $8.5\times$ ) of the optics used to image the output of the interferometer allowed the monitoring of the beams corresponding to the two arms of the interferometer. The magnification was such that nearly the entire intensity footprint of the x-ray laser beam was visible for both arms simultaneously. This is essential for the final alignment of the DGI because it provides information on the overlap, the intensity distribution, and quality of the fringes.

#### 4. Picosecond-Resolution Plasma Probing

To demonstrate soft-x-ray laser interferometry with picosecond resolution the DGI was combined with a transient 14.7-nm Ni-like Pd soft-x-ray laser.<sup>6</sup> The soft-x-ray laser was pumped by two beams from a chirped-pulse amplification laser, the Compact Multipulse Terawatt (COMET) system at Lawrence Livermore National Laboratory (LLNL) that operates at 1054 nm. An x-ray laser output of a few tens of

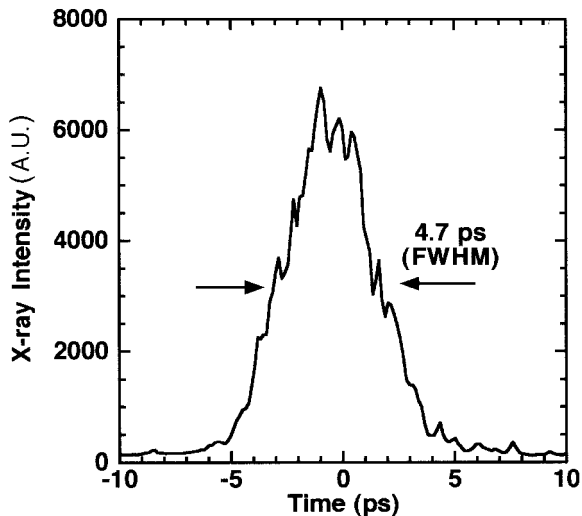


Fig. 2. Temporal profile of the Ni-like Pd 14.7-nm x-ray laser probe emitted from a 1-cm target and pumped by a 6.7-ps short pulse. Pulse shape is approximately Gaussian with 4.7 ps (FWHM).

microjoules was achieved by the optical pumping of a polished Pd target with a sequence of a 600-ps-long pulse ( $2 \text{ J}$ ,  $2 \times 10^{11} \text{ W cm}^{-2}$ ) and a 5-J energy 6.7-ps or 13-ps (FWHM) short pulse at an incidence intensity of  $6 \times 10^{13}$  and  $3 \times 10^{13} \text{ W cm}^{-2}$ , respectively. Traveling-wave line-focus excitation was achieved with a reflection echelon that consists of seven flat mirror segments placed before the focusing optics. Each mirror segment was offset by 0.12 cm to introduce the traveling wave toward the output of the laser with a delay of 7.7 ps per step. This results in a phase velocity ( $c$ ) along the line-focus length and ensures that peak gain conditions are experienced by the propagating x-ray laser photons. The horizontal angular divergence of the soft-x-ray laser was measured to be 2.8 mrad. The near-field and far-field beam characteristics were studied, and the laser parameters were optimized to obtain beam properties suitable for performing interferometry. It was decided to relay image the x-ray laser exit pattern from the end of the Pd target to the target plane inside the interferometer. This made the x-ray laser beam alignment insensitive to shot-to-shot variation in the deflection angle exiting the Pd plasma. Beam-pointing stability was better than  $25 \mu\text{rad}$ . This was achieved with a spherical  $0^\circ$  Mo-Si multilayer-coated mirror with 11.75-cm focal length at the end of the Pd plasma and an encoded flat  $45^\circ$  Mo-Si multilayer-coated mirror to point the x-ray beam onto the first interferometer grating, G1. The temporal properties of the x-ray laser have been recently measured with a fast-x-ray streak camera under the same laser-pumping conditions as those of the interferometry experiments.<sup>24</sup> Figure 2 shows a sample streak lineout with an x-ray pulse duration of 4.7 ps (FWHM) with an approximately Gaussian shape for a 6.7-ps short pump pulse. For saturated x-ray laser output the x-ray duration is typically in the range of

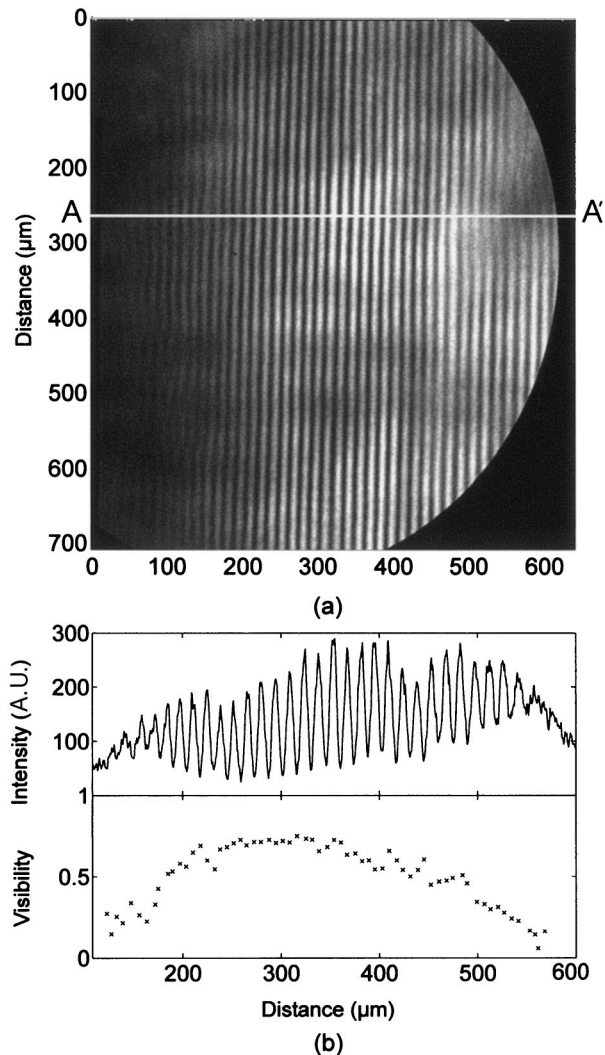


Fig. 3. (a) Interferogram obtained without the plasma present, (b) intensity and fringe visibility plots versus the distance away from the target surface between points A and A'.

4.5–5.2 ps. With the longer 13-ps pumping pulse, the measured x-ray duration is slightly longer at 5.9 ps.<sup>24</sup> Therefore the interferograms obtained with this setup have picosecond resolution, determined by the pulse duration of the soft-x-ray laser beam. This short pulse duration permits the acquisition of “snapshots” of the rapidly evolving plasma, overcoming the blurring of interference fringes that occur when the electron-density profile changes significantly during the duration of the probe pulse. The combination of the robust grating interferometer with the relatively high-repetition-rate picosecond soft-x-ray laser (1 shot every 4 min) permitted the acquisition of sequences of interferograms that map the evolution of the electron-density distribution in high-density laser-created plasmas.

Figure 3(a) shows a typical “reference” interferogram obtained without the plasma present. Figure 3(b) shows the fringe intensity as a function of the position away from the target, taken along the

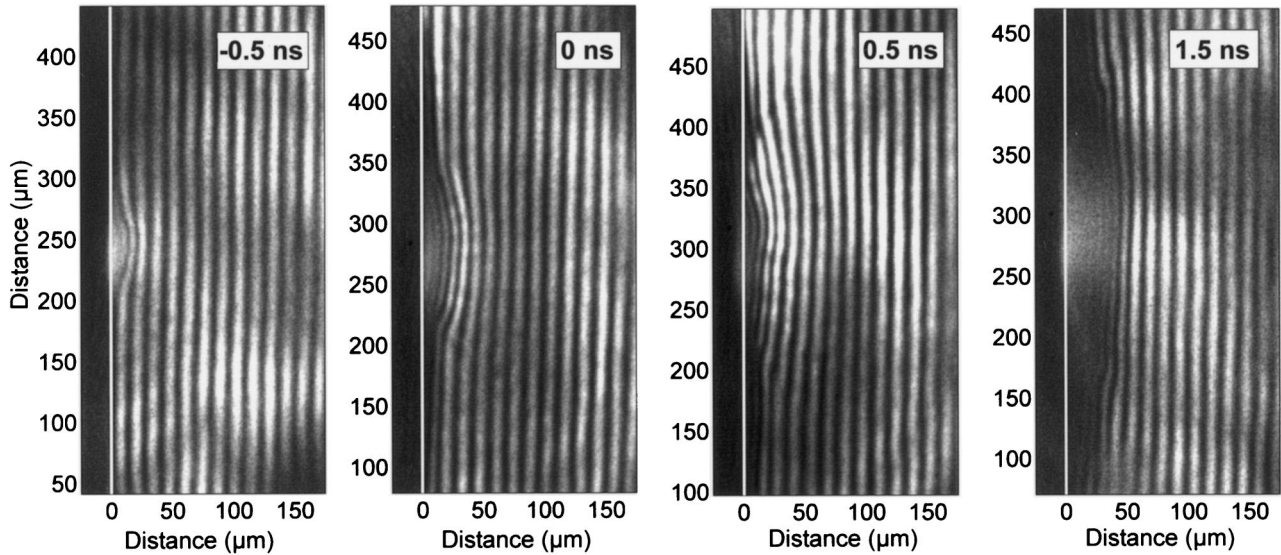


Fig. 4. Interferograms showing the evolution of a Ti plasma heated with a 600-ps, 1.1-J, 20- $\mu\text{m}$ -wide  $\times$  3.1-mm-long line focus. The times shown are measured from the peak of the heating pulse. The targets are 1 mm long.

dashed line between points A and A'. Some variation in intensity is visible because of mode structure within the x-ray laser beam. However, the visibility  $V = (I_{\text{max}} - I_{\text{min}})/(I_{\text{max}} + I_{\text{min}})$  calculated from this plot, and shown in Fig. 3(b), is excellent, with regions with over 0.8 visibility observed. Taking into account that for plasma-probing experiments good intensity is also needed to overcome absorption and intense plasma self-emission, this interferogram shows that the region suitable for plasma diagnostics is at least  $300 \mu\text{m} \times 700 \mu\text{m}$ . Plasma probing was achieved by the generation of a laser-produced plasma at a position halfway between the elongated mirror (L1) and the second grating (G2) along the trajectory of the zero-order arm of the interferometer (location marked as "Target" in Fig. 1). The targets were mounted on a motorized manipulator that allowed motion along all three axes. The rotation around the vertical axis was also controlled by a stepper motor to facilitate the alignment of the target

surface parallel to the x-ray probe beam. This angular alignment was better than  $0.25^\circ$  and reduced the shadowing of the fringes by a 1-mm-long target to  $2 \mu\text{m}$ . The rotations around the axis parallel and perpendicular to the target surface were also motorized to allow alignment with respect to the heating beam. The plasma was generated with a 1- $\omega$  (1054-nm) wavelength, 40-mm-diameter beam from the COMET laser, which provided up to 3 J of energy in 600-ps (FWHM) pulses. Because the same oscillator was used to generate both the plasma-heating beam and the soft-x-ray laser-pump beams, the laser pulses were well synchronized in every shot, with negligible jitter. A delay line on the plasma-forming beam allowed the relative timing to be changed so that the x-ray laser beam could probe the plasma at different times. An  $\sim 20\text{-}\mu\text{m}$ -wide, 3.1-mm-long line focus was generated on the target surface by a combination of a 200-cm focal-length cylindrical lens and a 30-cm focal-length off-axis

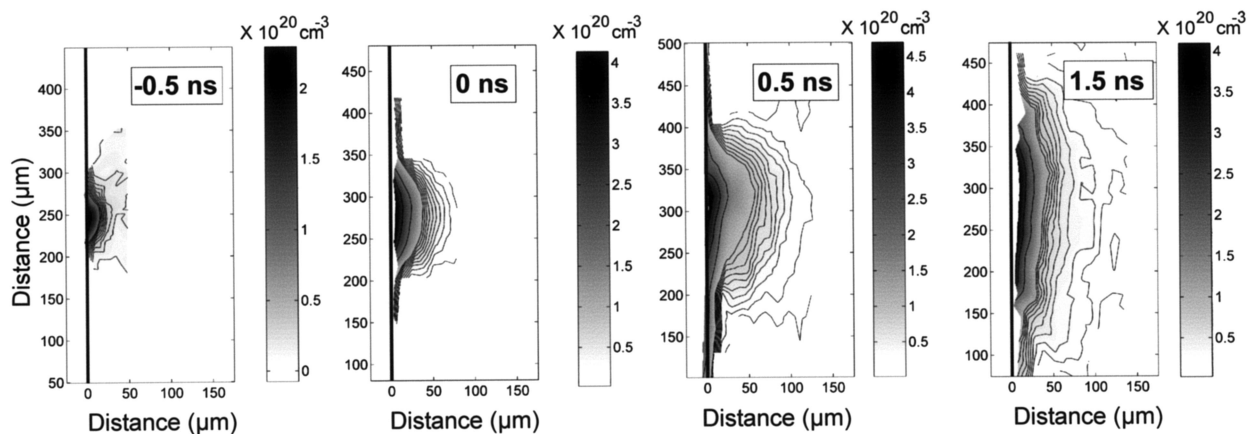


Fig. 5. Electron-density maps obtained from the interferograms shown in Fig. 4. The contour density lines represent a one-digit step.



paraboloid. The 1-mm-long targets were overfilled to obtain a uniform heating of the plasma. We measured the line-focus size and homogeneity by imaging the plasma-heating beam at the target plane with a through imaging system consisting of an achromatic lens and a series of relay mirrors that redirected the beam to a CCD camera. To limit the amount of plasma self-emission collected by the imaging CCD a 1-mm pinhole (not shown in Fig. 1) was placed between G2 and IM. The pinhole reduced the collection angle of the imaging system, thus reducing the amount of plasma x-ray self-emission recorded. To further block the stray optical light from the plasma-forming laser and from the plasma, a 2000-Å Zr + 1000-Å polyimide (C<sub>22</sub>H<sub>10</sub>N<sub>2</sub>O<sub>5</sub>) filter was placed in front of the CCD camera.

Figures 4(a)–4(d) show a sequence of interferograms that describe the evolution of a 1-mm-long plasma generated by the heating of a flat Ti target with the line-focus beam described above. The interferograms correspond to time delays of –0.5, 0, 0.5, and 1.5 ns measured with respect to the peak of the 600-ps heating laser pulse. Figure 4(a) corresponds to a time shortly after the initiation of the plasma. In the subsequent three frames of the evolution, plasma expansion is observed to have a significant component along the target surface direction, a characteristic that emphasizes its two-dimensional nature. Figure 5 shows the calculated density maps obtained from the interferograms in Fig. 4. Figure 5, third frame from the left, which corresponds to 0.5 ns after the peak of the 600-ps heating laser pulse, shows a maximum density of  $4.5 \times 10^{20} \text{ cm}^{-3}$  measured at a distance of 2 μm from the original target surface. A second type of target investigated was a groove in Al 100 μm wide, 200 μm deep, and 1 mm in length, as shown in the reference interferogram in Fig. 6(a). Beam 3 of the COMET laser was used to heat the bottom of the groove with 3 J in a tight ~12-μm-wide, 3.1-mm-long line focus. The shot shown in Fig. 6(b) illustrates an interferogram obtained at 1.25 ns after the peak of 600-ps heating laser pulse. The evolution of the plasma inside the groove has different characteristics from those corresponding to a flat target. The large and rapid lateral expansion of the plasma is constrained by the groove walls, forcing the plasma toward the center of the groove. The local maximum on axis can be interpreted as the collision of plasma arising from the walls. The electron-density map, Fig. 6(c), shows this axis-enhanced density. This example illustrates that picosecond soft-x-ray laser probes create the opportunities to study collisions and stagnation in large scale plasmas. A more complete study of the evolution of these plasmas will be published separately.

We constructed two-dimensional maps of the electron density by measuring the number of fringe shifts for different positions on the interferograms. For the axially uniform plasma of length  $L$  discussed

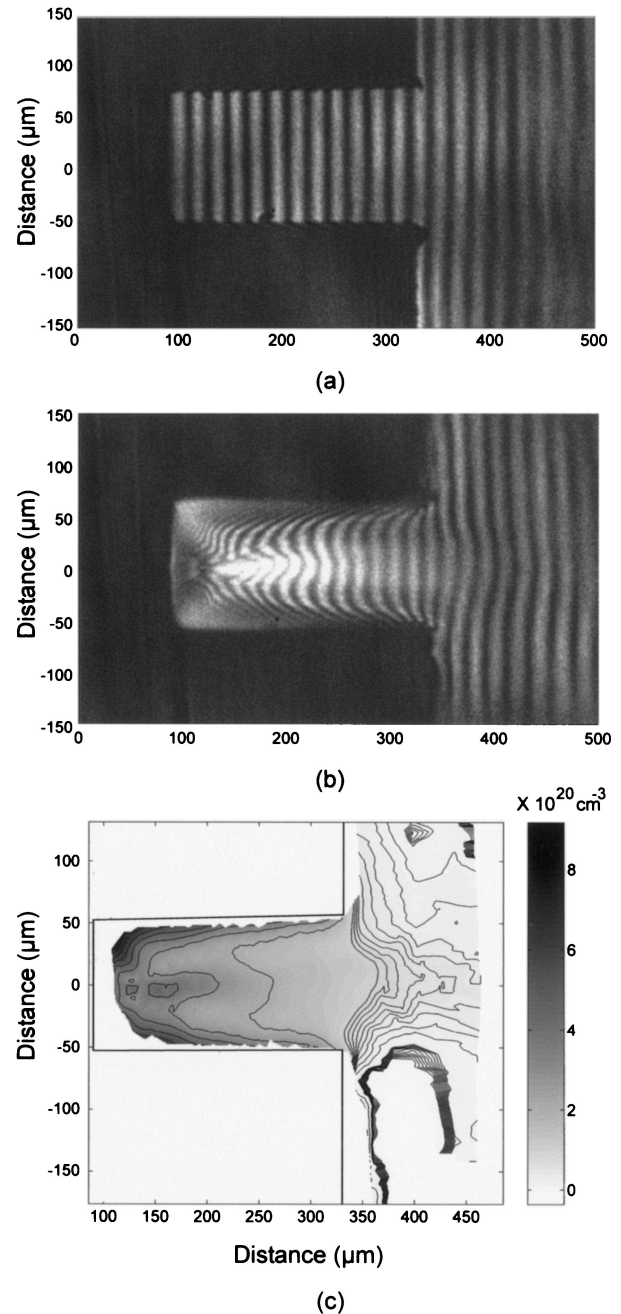


Fig. 6. (a) Reference interferogram showing a 100 μm × 200 μm Al groove target; (b) interferogram taken at 1.25 ns from the peak of the 600-ps, 3-J, line-focus plasma heating beam into the groove target; (c) electron-density map obtained from the interferogram in part (b) showing a maximum density of  $\sim 9 \times 10^{20} \text{ cm}^{-3}$  measured near the walls.

herein, the fringe shifts  $N_{\text{fringe}}$  observed in the interferograms are associated with a plasma electron density by<sup>25</sup>

$$N_{\text{fringe}} = \frac{\delta\phi}{2\pi} = \frac{1}{\lambda} \int_0^L (1 - n_{\text{ref}}) dl \approx \frac{n_e}{2n_{\text{crit}}} \frac{L}{\lambda},$$

where  $\delta\phi$  is the phase shift and the index of refraction  $n_{\text{ref}} = (1 - n_e/n_{\text{crit}})^{1/2}$  is a function of the electron

density  $n_e$  and the critical density  $n_{\text{crit}} = 1.1 \times 10^{21} \lambda^{-2}$  (in inverse cubic centimeters for the probe laser wavelength  $\lambda$  in micrometers). It is useful to express the electron density as a function of the observed fringe shifts:  $n_e = 2.2 \times 10^{21} N_{\text{fringe}}/\lambda L$ , where  $L$  and  $\lambda$  are expressed in micrometers. For the 14.7-nm wavelength of the probe laser and 1-mm length of the plasmas discussed herein, one fringe shift corresponds to a density of  $1.5 \times 10^{20} \text{ cm}^{-3}$ . In principle the minimum density increment  $\Delta n_e$  that can be measured depends on the minimum detectable fringe shift. If the fringes were perfectly straight the  $\sim 30$  pixels between lines in the interferograms shown in Fig. 6 would correspond to an error in the determination of the plasma electron density of  $\Delta n_e \sim 2.5 \times 10^{18} \text{ cm}^{-3}$ . However, in our case, undulations in the fringes that are due to the mode structure of the laser that varies from shot to shot limit the accuracy with which the reference fringes can be determined, increasing the uncertainty. An estimated uncertainty of 10%–20% in the determination of the reference fringes for the case of the 1-mm-long plasma results in an error of  $1.5\text{--}3 \times 10^{19} \text{ cm}^{-3}$  in the electron density. An additional phenomenon that can introduce errors in plasma-probing experiments is the extent to which the probe beam is deflected by refraction in the plasma medium.<sup>26</sup> The large density gradients encountered in laser-created plasmas close to the target can produce significant steering of the probe beam away from the highest-density regions. Knowledge of the extent and effect of refraction is therefore an important consideration for accurate analysis of the data. A grid reflectometry study was performed with the DGI<sup>27</sup> to estimate these refraction effects in 1-mm-long plasmas such as those investigated herein. That study showed that the present data can be analyzed without the need of a correction for refraction. Furthermore, refraction calculations, performed with the measured electron-density profile at the peak of the heating beam, show that close to the target surface the probe beam is deflected less than 1  $\mu\text{m}$ . This is in contrast with the use of an ultraviolet laser probe (e.g., the fourth harmonic of YAG, 266 nm), whose beam would have been strongly refracted away from the region close to the target shortly after entering the 1-mm-long plasma, making the probing of that region unfeasible.

## 5. Conclusions

Interferometry of dense plasmas at a wavelength of 14.7 nm has been demonstrated with picosecond resolution. The combined picosecond resolution and ultrashort wavelength of this technique has the potential for extending plasma interferometry significantly beyond the limits of current methods. The instrumentation developed for this purpose combines an amplitude-division interferometer that uses diffraction gratings as beam splitters with the 14.7-nm output of the Ni-like Pd transient soft-x-ray laser. The grating interferometer combines the advantages of excellent fringe visibility over a large area with high throughput and good resistance to damage by

the plasma. Several hundred plasma shots were performed with laser heating energies of up to 150 J without any observable damage or deterioration on the image quality. Densities up to  $4.5 \times 10^{20} \text{ cm}^{-3}$  were measured at distances as short as 2  $\mu\text{m}$  from the target in different types of millimeter-size line-focus laser-created plasmas. The instrumentation and methodology developed are scalable to significantly shorter wavelengths, and constitute a promising scheme for extending interferometry to the study of very dense plasmas such as those investigated for inertial confinement fusion.

The authors thank Albert Osterheld of LLNL for continued support of this work. In addition, the authors are grateful to Ronnie Shepherd and Rex Booth of LLNL for their help in the measurement of the x-ray laser-pulse duration. This research was sponsored by the National Nuclear Security Administration under the Stewardship Science Academic Alliances program through the U.S. Department of Energy research grant DE-FG03-02NA00062. Part of this work was performed under the auspices of the U.S. Department of Energy by the University of California, LLNL, through the Institute of Laser Science and Application, under contract No. W-7405-Eng-48. This work made use of Engineering Research Centers Facilities supported by the National Science Foundation under award No. EEC-0310717. The Colorado State University researchers also gratefully acknowledge the support of the W. M. Keck Foundation.

## References

1. T. P. Hughes, *Plasma and Laser Light* (Wiley, New York, 1975).
2. R. A. Alpher and D. R. White, "Optical Interferometry," in *Plasma Diagnostic Techniques*, R. H. Huddlestone and S. L. Leonard, eds. (Academic, New York, 1965), pp. 431–476.
3. L. B. Da Silva, T. W. Barbee, Jr., R. Cauble, P. Celliers, D. Ciarlo, S. Libby, R. A. London, D. Matthews, S. Mrowka, J. C. Moreno, D. Ress, J. E. Trebes, A. S. Wan, and F. Weber, "Electron density measurements of high density plasmas using soft x-ray laser interferometry," *Phys. Rev. Lett.* **74**, 3991–3994 (1995).
4. P. Celliers, F. Weber, L. B. Da Silva, T. W. Barbee, Jr., R. Cauble, A. S. Wan, and J. C. Moreno, "Fringe formation and coherence of a soft-x-ray laser beam illuminating a Mach-Zehnder interferometer," *Opt. Lett.* **20**, 1907–1909 (1995).
5. B. R. Benware, C. D. Macchietto, C. H. Moreno, and J. J. Rocca, "Demonstration of a high average power tabletop soft x-ray laser," *Phys. Rev. Lett.* **81**, 5804–5807 (1998).
6. J. Dunn, Y. Li, A. L. Osterheld, J. Nilsen, J. R. Hunter, and V. N. Shlyaptsev, "Gain saturation regime for laser-driven tabletop, transient Ni-like ion x-ray lasers," *Phys. Rev. Lett.* **84**, 4834–4837 (2000).
7. J. J. Rocca, C. H. Moreno, M. C. Marconi, and K. Kanizay, "Soft-x-ray laser interferometry of a plasma with a tabletop laser and a Lloyd's mirror," *Opt. Lett.* **24**, 420–422 (1999).
8. C. H. Moreno, M. C. Marconi, K. Kanizay, J. J. Rocca, Y. A. Uspenskii, A. V. Vinogradov, and Y. A. Pershin, "Soft-x-ray laser interferometry of a pinch discharge using a tabletop laser," *Phys. Rev. E* **60**, 911–917 (1999).
9. J. Filevich, K. Kanizay, M. C. Marconi, J. L. A. Chilla, and J. J. Rocca, "Dense plasma diagnostics with an amplitude-division



- soft-x-ray laser interferometer based on diffraction gratings,” *Opt. Lett.* **25**, 356–358 (2000).
10. R. F. Smith, J. Dunn, J. Nilsen, V. N. Shlyaptsev, S. Moon, J. Filevich, J. J. Rocca, M. C. Marconi, J. R. Hunter, and T. W. Barbee, “Picosecond x-ray laser interferometry of dense plasmas,” *Phys. Rev. Lett.* **89**, 065004 (2002).
  11. J. Y. Lin, G. J. Tallents, J. Zhang, A. G. MacPhee, C. L. S. Lewis, D. Neely, J. Nilsen, R. M. N. Pert, G. J. O’Rourke, R. Smith, and E. Wolfrum, “Gain saturation of Ni-like x-ray lasers,” *Opt. Commun.* **158**, 55–60 (1998).
  12. M. Born and E. Wolf, “Elements of the theory of diffraction,” in *Principles of Optics*, 7th ed. (Cambridge Univ. Press, Cambridge, England, 1999), pp. 412–516.
  13. M. Born and E. Wolf, “Elements of the theory of interference and interferometers,” in *Principles of Optics*, 7th ed. (Cambridge Univ. Press, Cambridge, England, 1999), pp. 286–411.
  14. F. Albert, D. Joyeux, P. Jaegle, A. Carillon, J. P. Chauvineau, G. Jamelot, A. Klisnick, J. C. Lagron, D. Phalippou, D. Ros, S. Sebban, and P. Zeitoun, “Interferograms obtained with an x-ray laser by means of a wavefront division interferometer,” *Opt. Commun.* **142**, 184–188 (1997).
  15. Ph. Zeitoun, F. Albert, P. Jaegle, D. Joyeux, M. Bousoukaya, A. Carillon, S. Hubert, G. Jamelot, A. Klisnick, D. Phalippou, J. C. Lagron, D. Ros, S. Sebban, and A. Zeitoun-Fakiris, “Investigation of strong electric-field induced surface phenomena by xuv laser interferometry,” *Nucl. Instrum. Methods Phys. Res. A* **416**, 189–191 (1998).
  16. L. B. Da Silva, T. W. Barbee, Jr., R. Cauble, P. Celliers, D. Ciarlo, J. C. Moreno, S. Mrowka, J. E. Trebes, A. S. Wan, and F. Weber, “Extreme-ultraviolet interferometry at 15.5 nm using multilayer optics,” *Appl. Opt.* **34**, 6389–6392 (1995).
  17. R. F. Smith, J. Dunn, J. R. Hunter, J. Nilsen, S. Hubert, S. Jacquemot, C. Remond, R. Marmoret, M. Fajardo, P. Zeitoun, and L. Vanbostal, “Longitudinal coherence measurement of a transient collisional x-ray laser,” *Opt. Lett.* **28**, 2261–2263 (2003).
  18. J. L. A. Chilla, J. J. Rocca, O. E. Martinez, and M. C. Marconi, “Soft x-ray interferometer for single-shot laser linewidth measurements,” *Opt. Lett.* **21**, 955–957 (1996).
  19. J. Filevich, J. J. Rocca, E. Jankowska, E. C. Hammarsten, K. Kanizay, M. C. Marconi, S. J. Moon, and V. N. Shlyaptsev, “Two-dimensional effects in laser-created plasmas measured with soft-x-ray laser interferometry,” *Phys. Rev. E* **67**, 056409 (2003).
  20. J. J. Rocca, E. C. Hammarsten, E. Jankowska, J. Filevich, M. C. Marconi, S. Moon, and V. N. Shlyaptsev, “Application of extremely compact capillary discharge soft x-ray lasers to dense plasma diagnostics,” *Phys. Plasmas* **10**, 2031–2038 (2003).
  21. M. Seminario, J. J. Rocca, R. A. Depine, B. Bach, and B. Bach, “Characterization of diffraction gratings by use of a tabletop soft-x-ray laser,” *Appl. Opt.* **40**, 5539–5544 (2001).
  22. Laser diode SDL-5401-GL by SDL (JDS Uniphase <http://www.jdsu.com>).
  23. Princeton Instruments PI-SX:1k. Roper Scientific, Inc., 3660 Quakerbridge Road, Trenton, N.J. 08619.
  24. J. Dunn, R. F. Smith, R. Shepherd, R. Booth, J. Nilsen, J. R. Hunter, and V. N. Shlyaptsev, “Temporal characterization of a picosecond laser-pumped x-ray laser for applications,” in *Soft X-Ray Lasers and Applications V*, E. E. Fill and S. Suckewar, eds., *Proc. SPIE* **5197**, 51–59 (2003).
  25. D. Attwood, “Soft x-rays and extreme ultraviolet radiation,” in *Physics of Hot Dense Plasmas* (Cambridge Univ. Press, Cambridge, England, 2000), p. 239.
  26. R. S. Craxton, F. S. Turner, R. Hoefen, C. Darrow, E. F. Gabl, and G. E. Busch, “Characterization of laser-produced plasma density profiles using grid image refractometry,” *Phys. Fluids B* **5**, 4419–4431 (1993).
  27. R. F. Smith, J. Dunn, J. Nilsen, J. R. Hunter, V. N. Shlyaptsev, J. J. Rocca, J. Filevich, and M. C. Marconi, “Refraction effects on x-ray and ultraviolet interferometric probing of laser-produced plasmas,” *J. Opt. Soc. Am. B* **20**, 254–259 (2003).